Hindawi
Mathematical Problems in Engineering
Volume 2021, Article ID 7422926, 15 pages
https://doi.org/10.1155/2021/7422926

Research Article

Comparative Study of the Near-Surface Typhoon Wind Profile Fitting between Offshore and Onshore Areas

Kai Wang,[1] Yun Guo,[2] and Xu Wang[1]

[1]*State Key Laboratory of Mountain Bridge and Tunnel Engineering, Chongqing Jiaotong University, Chongqing 400074, China*
[2]*Chongqing Vocational College of Transportation, Chongqing 402247, China*

Correspondence should be addressed to Xu Wang; xuwang@cqjtu.edu.cn

Received 24 September 2021; Revised 12 November 2021; Accepted 24 November 2021; Published 27 December 2021

Academic Editor: Andriette Bekker

The study of typhoon wind profiles, especially offshore typhoon wind profiles, has been constrained by the scarcity of observational data. In this study, the Doppler wind lidar was used to observe the offshore wind profiles during Super Typhoon Mangkhut and onshore wind profiles during Super Typhoon Lekima. Four wind profile models, including the power law, logarithmic law, Deaves–Harris (D-H), and Gryning, were selected in the height range of 0–300 m to fit the wind profile. The variations in the power exponent with the mean wind speed and roughness length were also analyzed. The results showed that the wind profiles fitted by the four models were generally in good agreement with the observed wind profiles with correlation coefficients greater than 0.98 and root mean square deviations less than 0.5 m s^{-1}. For the offshore case, the fitting degree of all wind profile models improved with increasing mean wind speed. Specifically, the D-H model had the highest fitting degree when the horizontal mean wind speed at 40 m was in the range of 8–25 m s^{-1}, while the log-law model had the highest fitting degree when the wind speed exceeded 30 m s^{-1}. For the onshore case, the fitting degree of the four wind profile models deteriorated with increasing mean wind speed, and the log-law model had the highest fitting degree in all wind speed intervals from 8 to 30 m s^{-1}. For both offshore and onshore cases, the power exponent was less affected by mean wind speed and increased with increasing roughness length, and the logarithmic empirical model proposed in this study could well characterize the relationship between the power exponent and roughness length.

1. Introduction

The wind profile, i.e., the vertical distribution of horizontal wind speed, has been the focus of much scholarly attention and research as one of the important bases for wind resistance design of flexible or dynamically sensitive building structures. On the basis of sorting out a large number of wind profiles, Davenport [1] found that the variation in horizontal wind speed with height was consistent with a power law function, and proposed the use of a power-law model to describe the wind profile in an approximate way. In the surface layer, the wind profile is mainly affected by the underlying surface roughness, friction velocity, atmospheric stability, and other parameters. When the atmospheric stability stratification is neutral, a log-law model describing the surface-layer wind profile can be derived based on the Buckingham π-dimensional analysis method [2] or mixed-length theory. In addition, based on the Monin–Obukhov similarity theory, a log-law model with a correction term for atmospheric stability could be obtained [3]. However, the log-law model can only accurately describe the wind profile in the surface layer. Above the surface layer, the shape of the wind profile is also influenced by the Coriolis parameter, baroclinicity, wind shear [4], and entrainment process near the top [5]. So the log-law model is no longer applicable. To describe the wind profile within the entire boundary layer, Deaves and Harris [6] modified the log-law model and proposed a wind profile model (i.e., the D-H model) applicable to the entire height range of the boundary layer. Subsequently, based on wind data observed at the 160 m mast of the Danish National Wind Turbine and the 250 m height TV tower in Germany, Gryning et al. [7] concluded

that the log-law model was only valid in the 50–80 m height range, with large deviations at higher heights. Therefore, a wind profile model that could describe the entire boundary layer was also derived based on a series of assumptions.

A typhoon is an intense mesoscale vortex with a very complex spatial structure, usually consisting of a low-pressure calm typhoon eye, a ring of maximum wind speed eye walls, and a number of spiral rainbands distributed radially within the boundary layer [8]. It causes severe damage to life and property in many areas due to the destructive winds, high surges, torrential rains, and severe flooding it produces. Therefore, it is essential to study the vertical distribution pattern of the horizontal wind speed under typhoon conditions. Due to the difference between the underlying surfaces of offshore and onshore areas, typhoon wind profiles may have different characteristics in offshore and onshore areas. In offshore areas, Power et al. [9] studied 331 strong wind profiles measured by GPS dropwindsonde near the eyewall of hurricanes in the Atlantic, and Eastern and Central Pacific basins from 1997 to 1999. The results showed that within the lower height of 200 m, the mean wind speed increases logarithmically with the height and reaches a maximum near the height of 500 m. This result is a good description of offshore wind profile characteristics during tropical cyclones. In the onshore area, Tamura et al. [10] used two sets of Doppler sodars to observe the boundary layer wind in the seaside and inland areas, compared the characteristics of the mean wind profile of the same storm under different terrain roughness, and performed power-law and log-law model fitting of mean wind profiles. The results showed that the mean wind profile is different between suburbs and cities, the power-law model can describe the mean wind profile in suburbs well and is suitable for the mean wind profile over cities, and the log-law model is more suitable for both city and suburban areas in the height range of 100–150 m. Wang et al. [11] used power-law, log-law and D-H models to fit the mean wind profile for wind speeds greater than 12 m s^{-1} at 10 m height based on data recorded from a wind observation tower in Pudong District (Shanghai) for Typhoon Meihua. The results show that the model-fitted wind profiles are in good agreement with the observed wind profiles. Li et al. [12] analyzed the mean wind profile characteristics in different sections of tropical cyclones by using the data of three typhoons observed from wind observation towers and Doppler sodars, and analyzed the influence of factors such as roughness length and mean wind speed on the mean wind profile characteristics. The results showed that the roughness length, mean wind speed, and different sections of typhoon have a significant influence on the characteristics of the mean wind profile. To compare the differences in offshore and onshore wind profiles during tropical cyclones, Giammanco et al. [13] investigated the characteristics of the offshore and onshore vertical wind profiles during tropical cyclones and their variation with storm-relative position, based on GPS dropwindsonde and WSR-88D (Weather Surveillance Radar-1988 Doppler) observations. The results indicated significant differences in the characteristics of the mean wind profiles in offshore and onshore areas. Based on the synchronized measurements from a Doppler radar wind profiler and an anemometer during 16 tropical cyclones at a coastal site in Hong Kong, He et al. [14] investigated the vertical profiles of horizontal mean wind speed and direction. The results showed that the mean wind profile below 500 m followed the logarithmic law for both hilly upwind terrain and open sea upwind terrain, and the fitting parameters of the log-law and power-law models in different reference speed groups increased with the mean boundary layer (MBL) speed, in which the friction velocity and power exponent increased linearly, while the roughness increased exponentially. However, the above studies lack a quantitative comparison of the typhoon wind profile fitting degree of the power law, logarithmic law, D-H, and Gryning models in offshore and onshore areas.

Due to its simple form and easy application, the power-law model has been used as the standard model to describe wind profiles in wind resistance design specifications of building structures in many countries [15–17]. The power exponent obtained by fitting the observed wind profile using a power-law model is an important parameter reflecting the shape of the wind profile. To investigate the factors affecting the power exponent, Ishizaki and Aerodynamics [18] analyzed the variation of wind profiles with mean wind speed and found that the power exponent decreases with increasing wind speed, independent of terrain roughness length. In contrast, by matching the logarithmic law with the power law, Panofsky and Dutton [19] showed that the power exponent can be estimated by the roughness length. Later, Song et al. [20] analyzed the influence of the roughness length of the underlying surface on the power exponent based on the records of six observation towers on three typhoons, and proposed an empirical power ratio formula between the power exponent and roughness length. However, in offshore and onshore areas, the factors affecting the power exponent need to be further explored by using more typhoon data, and the applicability and accuracy of the power exponent model proposed by Panofsky and Dutton [19] and Song et al. [20] need to be further verified in offshore and onshore areas.

There is a need to investigate and quantitatively compare the applicability of the power-law, log-law, D-H, and Gryning models under typhoon conditions in offshore and onshore areas, to verify the accuracy and applicability of the power exponent models proposed by Panofsky and Dutton [19] and Song et al. [20] in offshore and onshore areas, respectively, and to investigate whether there are more accurate and simple empirical models that can better describe the relationship between the power exponent and roughness length, thus providing a simple and effective method for estimating the power exponent from roughness length in typhoon-prone areas. This study is intended to investigate the applicability of four wind profile models in offshore and onshore areas based on Doppler wind lidar (DWL) observations of Super Typhoons Mangkhut and Lekima in offshore and onshore areas, respectively, and to analyze the variation in the power exponent with mean wind speed and roughness length in offshore and onshore areas, respectively. The results of this study will help to enhance the understanding of the differences between offshore and

onshore typhoon wind profiles and provide a reference for the typhoon resistance design of offshore wind turbines and onshore building structures.

The remainder of this paper is organized as follows. Section 2 briefly introduced Super Typhoon Mangkhut and Super Typhoon Lekima and the related information of observation records, including the path and intensity of typhoons, and detailed description of the observation sites and wind records. Section 3 describes the treatment of the observed data, including the description of four wind profile models and the selection of samples. Section 4 compares and analyzes the accuracy of four wind profile models in different wind speed intervals and height ranges in offshore and onshore areas. Section 5 analyzes the effect of mean wind speed as well as roughness length on the variation of power exponent in offshore and onshore areas, and proposed a new model that can accurately describe the relationship between roughness and power exponent. Finally, Section 6 comprises the results and discussion.

2. Typhoon and Observational Records

2.1. Typhoon Mangkhut and Typhoon Lekima. Super Typhoon Mangkhut was the 22nd tropical cyclone generated in the western North Pacific in 2018 (Figure 1(a)). On September 7, Mangkhut formed a tropical depression at 12 N, 170 E, and strengthened into a super typhoon on September 11. On the morning of September 15th, Mangkhut made its first landfall on Luzon Island in the Philippines. At the moment of landfall, the sustained wind speed in 1 min at a height of 10 m reached 70 m s^{-1}. After passing through Luzon, Mangkhut was downgraded to a severe typhoon and continued to move northwest. At approximately 15:00 on 16 September, Mangkhut made landfall again in Guangdong, China, with a 2-min sustained winds of 45 m s^{-1} at a height of 10 m at the time of landfall. Then, it continued to move inland and dissipated in the evening of 17 September.

Super Typhoon Lekima was the 9th tropical cyclone generated in the western North Pacific Ocean on August 4, 2019 (Figure 1(b)). It strengthened into a super typhoon on the evening of July 7 and made landfall in the coastal area of Wenling city, Zhejiang Province, China at 1:45 on October 10. At the time of landfall, the maximum wind force near the center was level 16 (52 m s^{-1}, super typhoon level). After passing through Zhejiang and Jiangsu provinces, Lekima moved into the western part of the Yellow Sea. At 20:50 on November 11, it made landfall again off the coast of Huangdao District, Qingdao city, Shandong Province, China, and finally crossed the Shandong Peninsula into the Bohai Sea.

Part of the best path of Mangkhut and Lekima provided by JTWC (Joint Typhoon Warning Center) is shown in Figure 1, and the time is Chinese Standard Time (CST = UTC + 8 h). The typhoon data for Mangkhut used in this study were the DWL wind records obtained from the observation site on the south side of Jinwan District, Zhuhai City, Guangdong from 19:00 on September 15, 2018 to 22:00 on September 17, 2019. The wind data for Lekima were the DWL wind records obtained from the observation site in Taizhou, Zhejiang from 00:00 on August 8, 2019 to 23:50 on August 10, 2019. The detailed description of the location of the observation sites and the wind records will be given in Section 2.2.

2.2. Observational Site and Records. The Jinwan observation site was located in the offshore area southeast of Sanzao town, Jinwan District, Zhuhai City, Guangdong Province, China (21.876325°N, 113.434503°E). The surrounding terrain of the observation site is shown in the upper right corner of Figure 1(a). The observation site was approximately 15 km from the north coastline and approximately 12 km from the northwest coastline. The east and south sides of the observation site were all offshore areas. When the typhoon center passed the observation site, the closest distance between the typhoon center and the observation site was approximately 44 km, and the intensity level of the typhoon at this time was the typhoon level.

The Taizhou observation site was located in a vacant lot on the east side of a football field at Hongjia Central Primary School in Jiaojiang District, Taizhou City, Zhejiang Province (28.6180°N, 121.4166°E). The surrounding terrain of the observation site is shown in the upper right corner of Figure 1(b). The eastern part of the site had a small building area and a large arable area, while the northern, western, and southern parts were densely populated with urban buildings. When the typhoon center passed the observation site, the closest distance between the typhoon center and the observation site was approximately 13 km, and the intensity level of the typhoon at this time was the typhoon level.

The DWL used in the study was a WindCube V2 pulsed-type lidar manufactured by Leosphere®. It can continuously measure the wind speed and direction, CNR (carrier-to-noise ratio), near-surface air temperature, relative humidity, and air pressure within height intervals of 0–300 m. Measurements were recorded at 12 different heights, including 40 m, 50 m, 70 m, 80 m, 90 m, 100 m, 110 m, 120 m, 140 m, 170 m, 190 m, and 210 m for Mangkhut and 40 m, 50 m, 70 m, 100 m, 130 m, 150 m, 180 m, 200 m, 230 m, 250 m, 270 m, and 290 m for Lekima. The measurement principle and calibration of the DWL can be found in [21]. The specifications of the DWL are shown in Table 1.

3. Data Processing Method

3.1. Wind Profiles Model

3.1.1. Power-Law Model. The power-law model was proposed by Davenport [1] based on the collation of a large number of wind profiles. Due to its simple form, it was used in many countries, including China, as a model for describing the vertical distribution of wind speed in wind resistance codes. The formula is

$$u(z) = u(z_1)\left(\frac{z}{z_1}\right)^{\alpha}, \tag{1}$$

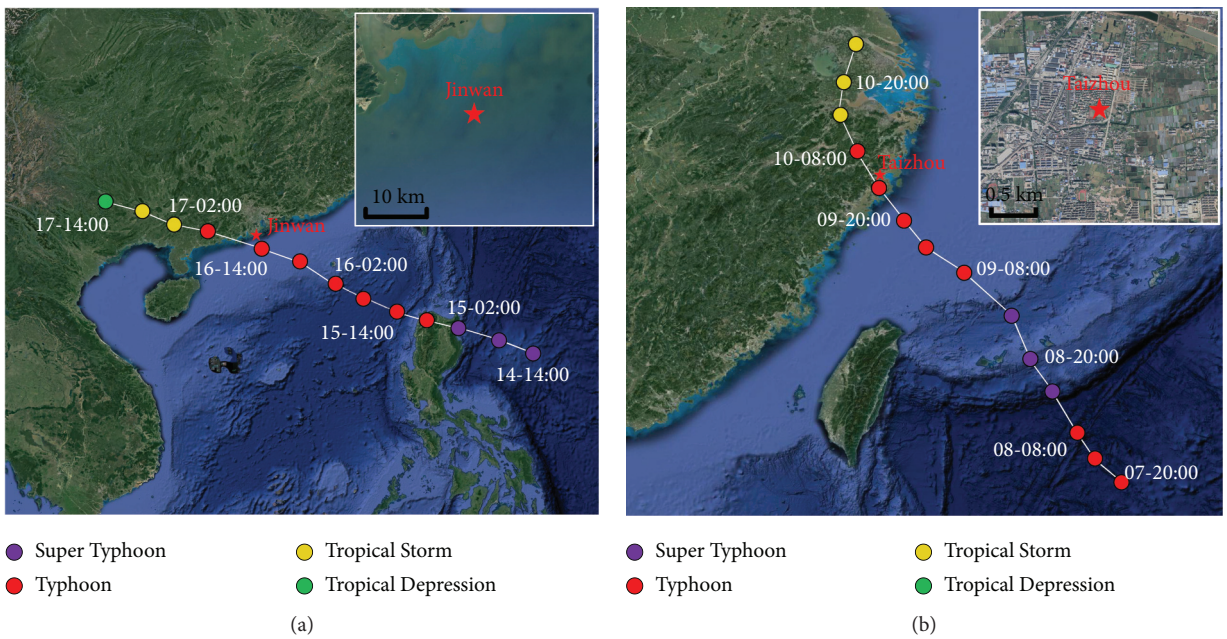

Figure 1: Best track of the typhoon and the exposure of the observation site, including (a) Mangkhut; (b) Lekima (in CST, or UTC + 80). The tropical cyclone intensity scale forms JTWC: Tropical Depression (10.8–17.1 m s^{-1}); Tropical Storm (17.2–32.6 m s^{-1}); Typhoon (32.7–61.2 m s^{-1}); Super Typhoon (61.2 m s^{-1}–).

Table 1: Specifications of the DWL.

Parameter	DWL (WindCube V2)
Measurement intervals	4–290 m
Number of measurement levels	12
Data sampling rate	1 Hz
Speed accuracy	0.1 m s^{-1}
Speed intervals	0–80 m s^{-1}
Direction accuracy	1°
Temperature intervals	−35°C to +45°C
Humidity intervals	0%–100% RH

where z is the height and $u(z)$ is the wind speed at height z, z_1 is the reference height, $u(z_1)$ is the wind speed at the reference height, and α is the power exponent.

3.1.2. Log-Law Model. According to the Monin–Obukhov theory of similarity [3], the wind profile could be described by the following equation:

$$u(z) = \frac{u_*}{\kappa}\left[\ln\frac{z}{z_0} - \psi\left(\frac{z}{L}\right)\right], \tag{2}$$

where κ is the von-Kármán constant, u^* is the friction velocity, z_0 is the roughness length, ψ is the Monin–Obukhov function, and L is the Monin–Obukhov length. In the neutral stability stratification, equation (2) can be simplified to

$$u(z) = \frac{u_*}{\kappa}\ln\frac{z}{z_0}. \tag{3}$$

This study intends to use the wind profile method [22] to calculate the roughness length. Under near-neutral conditions, equation (3) is generally used to fit the mean wind speed profile by the least square method, and the roughness length z_0 is calculated as one of the fitting parameters [20, 23].

3.1.3. Deaves–Harris Model. The D-H model was a model proposed by Deaves and Harris [6] as a refinement of the log-law model. It overcame the disadvantage that the log-law model could only describe surface layer wind profiles and wind profiles across the entire atmospheric boundary layer. The expressions are as follows:

$$u(z) = \frac{u_*}{\kappa}\left[\ln\frac{z}{z_0} + 5.75\frac{z}{h} - 1.88\left(\frac{z}{h}\right)^2 - 1.33\left(\frac{z}{h}\right)^3 + 0.25\left(\frac{z}{h}\right)^4\right], \tag{4}$$

where h is the height of the boundary layer, calculated by the following equation:

$$h = \frac{1}{\beta}\frac{u_*}{f}, \tag{5}$$

where β is the empirical parameter, generally taken as 6, and f is the Coriolis parameter, related to the latitude of the observation site.

For a neutral atmosphere below 300 m altitude [11], equation (4) can be simplified as

$$u(z) = \frac{u_*}{\kappa}\left[\ln\left(\frac{z}{z_0}\right) + 34.5\frac{fz}{u_*}\right]. \tag{6}$$

3.1.4. Gryning Model. Due to the bias of the log-law model in describing the wind profile above a height of 100 m,

Gryning et al. [7] proposed a wind profile model that can describe the entire boundary layer. Under neutral conditions, the expressions are as follows:

$$u(z) = \frac{u_*}{\kappa}\left[\ln\left(\frac{z}{z_0}\right) + \frac{z}{L_{MBL,N}} - \frac{z}{h}\left(\frac{z}{2L_{MBL,N}}\right)\right], \quad (7)$$

$L_{MBL,N}$ is the total length scale under neutral conditions. The formula is

$$L_{MBL,N} = \frac{u_*}{[-2\ln(u_*/fz_0) + 55]f}. \quad (8)$$

3.2. Samples Selection. Based on the assumptions and investigations of Chen et al. [24] and He et al. [23] on the relationship between atmospheric stability and mean wind speed, this study assumed that atmospheric stability is near neutral when $U(40)$ exceeded $8\,\mathrm{m\,s^{-1}}$. Therefore, only samples of strong winds observed in offshore and onshore areas during Typhoons Mangkhut and Lekima were selected for study. Here, the samples of offshore and onshore strong winds were considered to be wind profiles with $U(40)$ greater than $8\,\mathrm{m\,s^{-1}}$. Finally, the Lekima wind data at an altitude of 290 m were not selected because they were deemed invalid.

4. Study on the Characteristics of Mean Wind Profile and the Applicability of Wind Profile Models

A single wind profile hardly reflects the general pattern due to the presence of convection, gusts, turbulence, and other uncertainties [25]. As a result, a large number of studies have been conducted using composite wind profiles [9, 13, 14, 25–27]. In this study, the mean wind profile characteristics and the fitting of the mean profile models were also studied using a composite wind profile approach, i.e., averaging the horizontal wind speeds of all 10 min mean wind profiles at the same height.

4.1. The Effect of Mean Wind Speed on Wind Profile. To investigate the effect of mean wind speed on the characteristics of mean wind profiles and the applicability of wind profile models, Power et al. [9] and He et al. [14] grouped observed wind profiles according to mean boundary layer (MBL) wind speed, defined as the mean wind speed of all profile observations below 500 m. Tamura et al. [26] conducted a grouping study based on the mean wind speed at 17 heights in the 50–340 m height intervals. Wang et al. [11] grouped the observed wind profiles based on the mean wind speed at a height of 10 m. This study proposes to group studies based on $U(40)$. All 10 min mean wind profiles of Mangkhut were divided into five groups with wind speeds in the range of 8–17.2 $\mathrm{m\,s^{-1}}$, 17.2–20 $\mathrm{m\,s^{-1}}$, 20–25 $\mathrm{m\,s^{-1}}$, 25–30 $\mathrm{m\,s^{-1}}$, and 30–35 $\mathrm{m\,s^{-1}}$. Similarly, all 10 min mean wind profiles for Lekima were divided into four groups with wind speeds in the range of 8–17.2 $\mathrm{m\,s^{-1}}$, 17.2–20 $\mathrm{m\,s^{-1}}$, 20–25 $\mathrm{m\,s^{-1}}$, and 25–30 $\mathrm{m\,s^{-1}}$. Figure 2 shows the 10 min mean wind speed and mean wind direction time history curve at 40 m height for Mangkhut and Lekima. The time history curve of the mean wind speed of Mangkhut has a single-peaked distribution, and the maximum wind speed can reach 34.75 $\mathrm{m\,s^{-1}}$. During the period from 12:00 to 17:50 on 16 September, the mean wind speed was approximately 30 $\mathrm{m\,s^{-1}}$ and the mean wind direction changed by approximately 156.2°. When the typhoon center passed the offshore observation site, the mean wind speed reached 30.94 $\mathrm{m\,s^{-1}}$ and the mean wind direction was 86.1°. Lekima's wind speed time history curve also shows a single-peaked distribution, with the maximum wind speed reaching 27.43 $\mathrm{m\,s^{-1}}$. Between 23:00 on 9 August and 05:30 on 10 August, the mean wind speed was basically greater than 17.2 $\mathrm{m\,s^{-1}}$, and the mean wind direction changed by approximately 95.09°. When the typhoon center passed the onshore observation point, the mean wind speed reached 21.12 $\mathrm{m\,s^{-1}}$, and the mean wind direction was 108.53°.

Figure 3 shows the variation curves of the mean wind speed with height in different wind speed intervals. The mean wind speed at each height was normalized in this study using $U(40)$. Figure 3(a) shows the normalized wind profile of Lekima observed in offshore areas. There are significant differences in the normalized wind profiles within the different wind speed intervals, and the mean wind speed shows different increasing trends with increasing height. Specifically, in the 17.2–35 $\mathrm{m\,s^{-1}}$ wind speed interval, the normalized wind profiles below 100 m height are close to coincident, while above 100 m height, the curves gradually diverge, with the differences becoming more pronounced with increasing height. Figure 3(b) shows the normalized wind profiles of Typhoon Lekima observed in the onshore area. In the three different wind speed intervals from 8 to 25 $\mathrm{m\,s^{-1}}$, the normalized wind profiles up to 70 m height largely coincide, while the differences between the normalized wind profiles in each wind speed interval gradually start to appear as the height increases; in the high wind speed intervals of 25–30 $\mathrm{m\,s^{-1}}$, the normalized wind profiles differ more significantly from the other relatively low wind speed intervals.

In addition, by comparing the wind speed ratios ($U/U(40)$) at the same wind speed interval and height at the offshore and onshore observation sites, the rate of change of the wind speed ratio with height was much greater at the onshore site than offshore site, for example, the wind speed ratio in the 17.2–20 $\mathrm{m\,s^{-1}}$ wind speed intervals was approximately 1.1 at the offshore site at 100 m height, while the wind speed ratio at the onshore site in the same conditions was approximately 1.3.

To compare the accuracy and applicability of the four wind profile models—power law, log law, D-H, and Gryning—in describing the wind profile in different wind speed intervals, the least squares method was applied to fit the observed wind profiles in several wind speed intervals. Figure 4 shows the observed wind profiles of Mangkhut observed at the offshore site and the model-fitted wind profiles of the four models. Under typhoon conditions, the overall fitting degrees of the four models were generally better, but there were minor differences. As the mean wind speed increased, the wind profile model fit the observed wind speed profile progressively better.

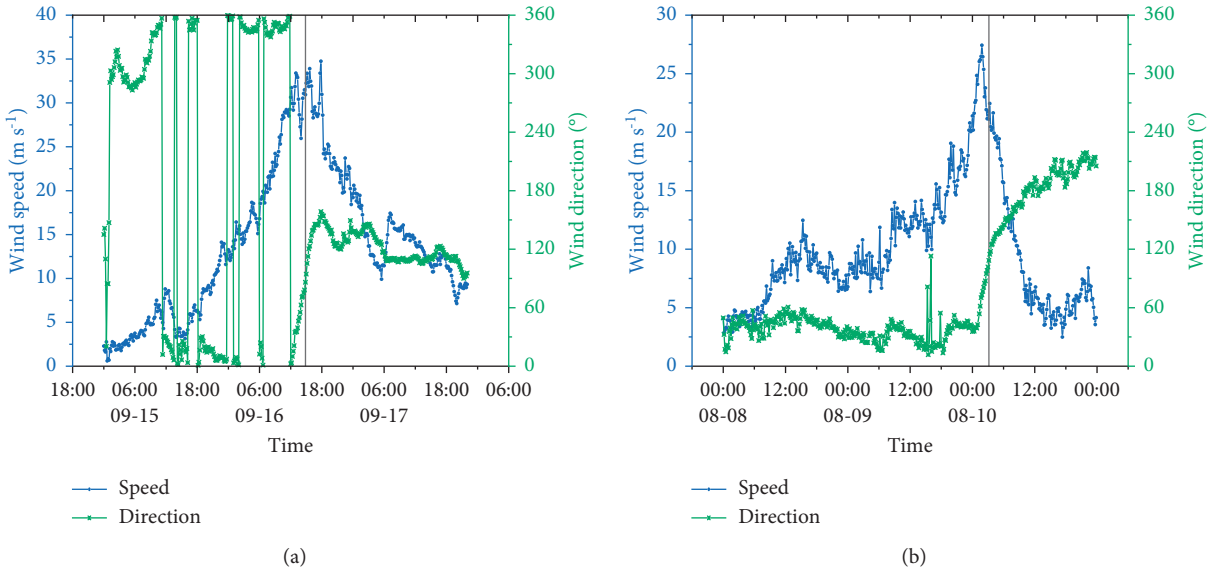

Figure 2: Time histories of 10 min mean wind speed and direction at 40 m height during the passage of (a) Mangkhut and (b) Lekima. The black vertical line represents the moment of the typhoon center passing the observation site.

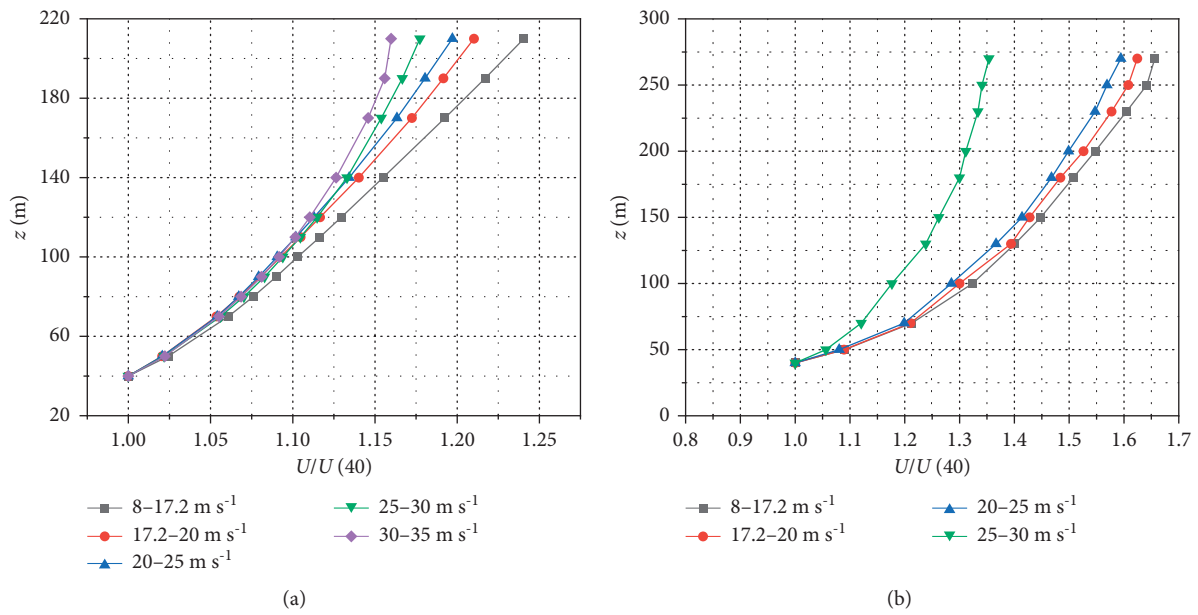

Figure 3: Mean wind profiles by $U(40)$ group in (a) typhoon Mangkhut and (b) typhoon Lekima.

To quantify the degree of the four wind profile models on fitting the observed wind profiles in different wind speed intervals, the root mean square error (RMSE) and the correlation coefficient (R) were calculated between the gradient wind speed values of the observed wind profiles and the gradient wind speed values fitted by the four wind profile models, and these two parameters were used as evaluation indicators to determine their applicability. Figure 5 shows the point line plot of RMSE and R between the four model-fitted wind profiles and the observed wind profile in offshore areas. In general, under strong wind conditions, the differences in R values between the four model wind profiles and the observed wind profiles were very small, which were greater than 0.99. The RMSEs were slightly different, but all were less than 0.18 m s^{-1}, so the overall fitting degree was high. Specifically, as the mean wind speed increased, the RMSE of the four wind profile models showed an overall decreasing trend, while the R gradually increased. When $U(40)$ was in the interval of 8–25 m s^{-1}, the RMSE between the power-law and log-law model-fitted wind profiles and the observed wind profile reached the maximum, while the RMSE between the D-H model-fitted wind profiles and the observed wind speed profile was the minimum. R between the D-H model-fitted wind profiles and the observed wind

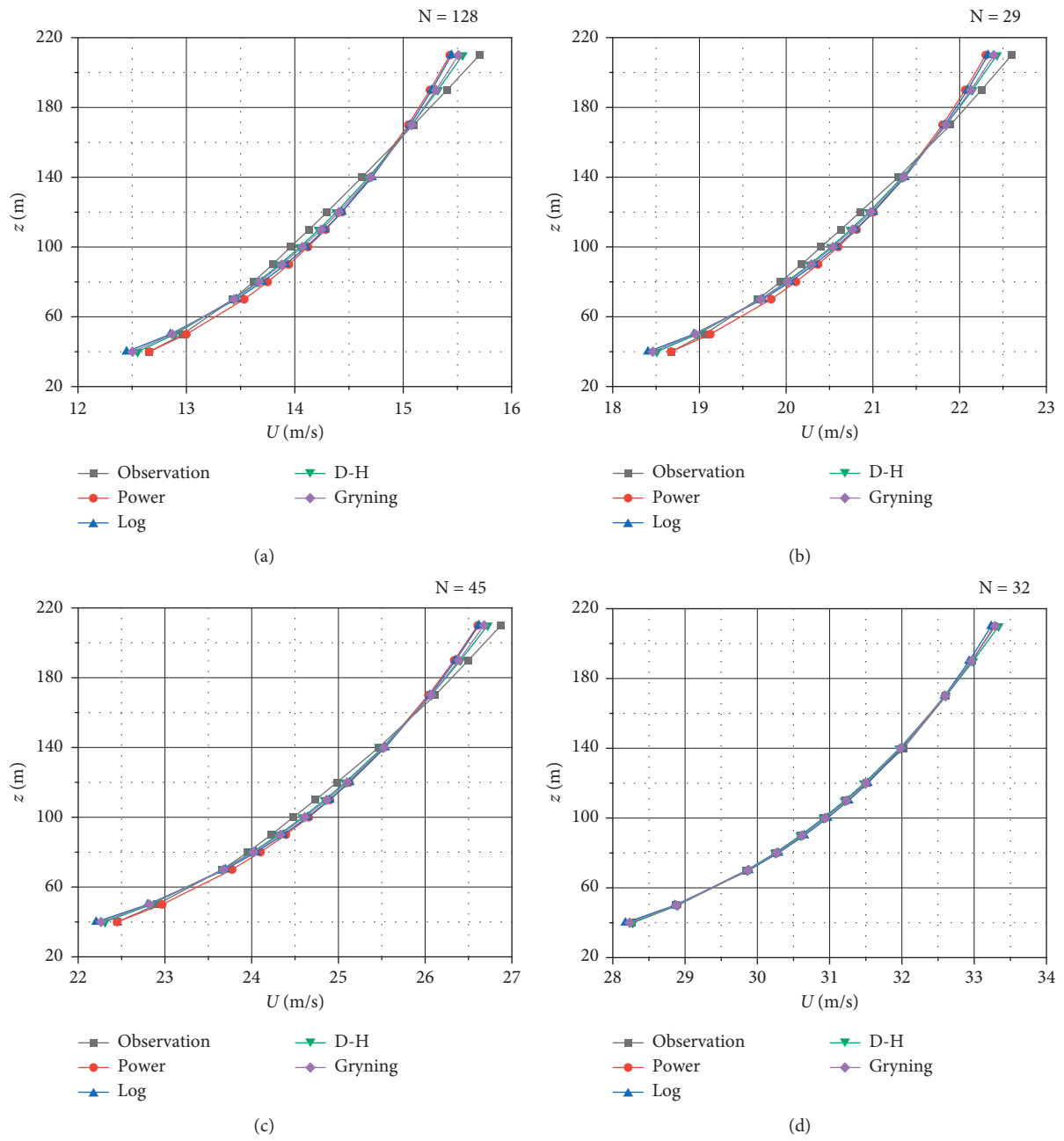

Figure 4: Continued.

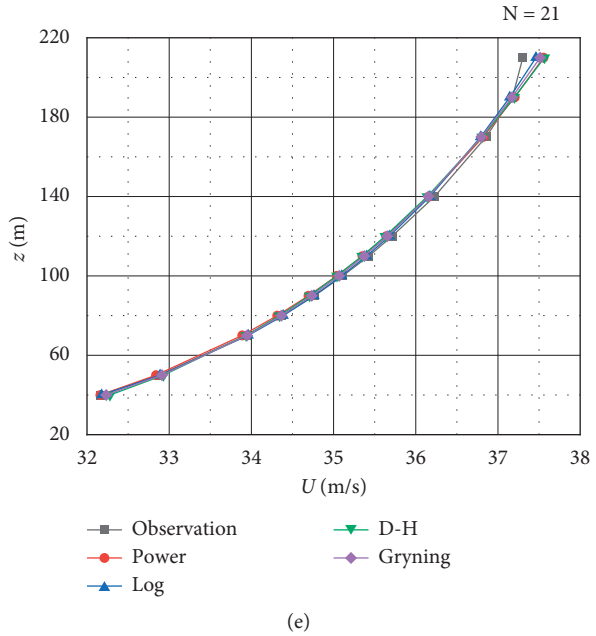

Figure 4: Mean wind profiles by $U(40)$ group, compared with model-fitted wind profiles in typhoon Mangkhut. (a) 8–17.2 m s^{-1}; (b) 17.2–20 m s^{-1}; (c) 20–25 m s^{-1}; (d) 25–30 m s^{-1}; and (e) 30–35 m s^{-1}.

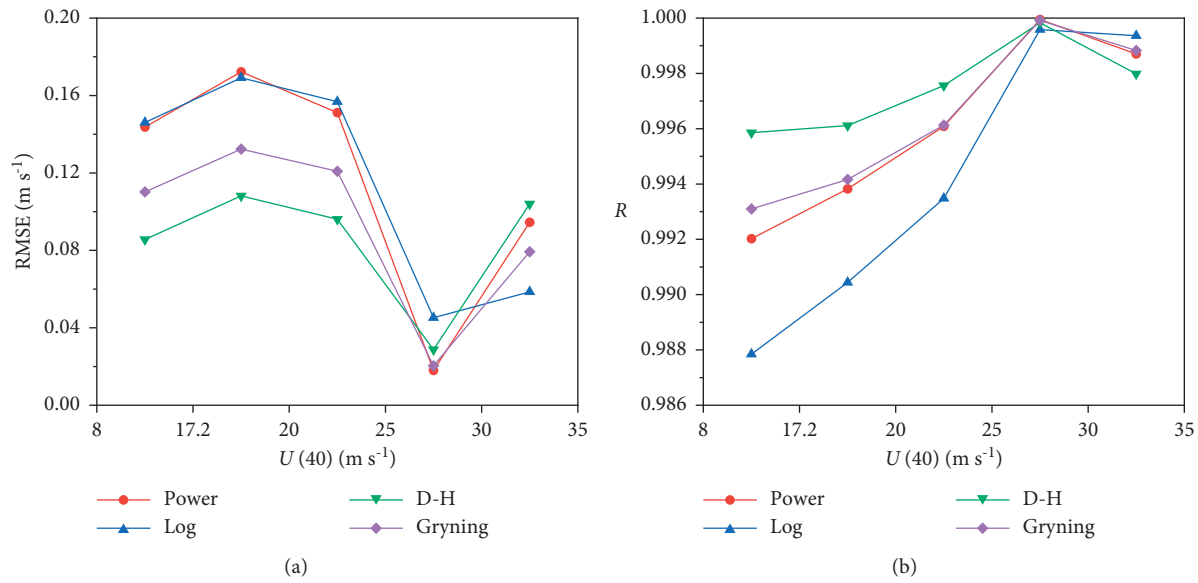

Figure 5: The error between the observed gradient wind speed value and the model-fitted gradient wind speed value by U (40) group in typhoon Mangkhut.

profile was the maximum, and the log-law model was the minimum. In addition, the RMSE and R of the four model-fitted wind profiles were basically consistent with the observed wind profiles in the wind speed interval of 25–30 m s^{-1}, and there was little difference in the fitting degree. In the 30–35 m s^{-1} interval, RMSE D-H > power law > Gryning > logarithmic law, and R logarithmic law- > power law = Gryning > D-H.

According to the above analysis, with the increase in the mean wind speed, the fitting degree of the four wind profile models on the observed wind profile gradually improved. In the wind speed intervals of 8–25 m s^{-1}, the D-H model describes the observed wind profile the best, and when $U(40)$ exceeded 30 m s^{-1}, the applicability of the log-law model became the best among the four models.

The applicability of the offshore wind profile models in different wind speed intervals has been analyzed and quantitatively compared above. To compare the wind speed profile characteristics and the applicability of the wind profile models in offshore and onshore areas, this study

analyzed the wind profile of Lekima observed in the onshore area, and the analysis was consistent with the method and content of the analysis of the Mangkhut. Figure 6 shows the observed wind profiles of Lekima in different wind speed intervals observed in the onshore area and four model-fitted wind profiles. Consistent with the analysis results of the offshore wind profile, the four wind profile models still had generally high-fitting degrees on the observed wind profile. In the same wind speed intervals, it is apparent that the applicability of the wind profile model in offshore areas was better than that in onshore areas. It is worth noting that in the wind speed intervals of 25–30 m s^{-1}, the observed wind speed profile deviated greatly from the model-fitted wind profile. The possible reason is that there were fewer samples in this wind speed interval, which leads to poor representativeness of the composite wind profile synthesized in this wind speed interval.

The following is a quantitative analysis of the fitting degree of the wind profile models on the observed wind profile in different wind speed intervals, and the analysis method is the same as that of Mangkhut. Figure 7 shows a dotted line plot of RMSE and R between the four model-fitted wind profiles and the observed wind profile. Within all wind speed intervals, the RMSE between the power-law model wind profile and the observed wind profile was the largest, R the smallest, and the fitting degree the lowest. The D-H model and Gryning model had similar fitting degrees, which were in the middle, and the log-law model had the highest fitting degree. In addition, with the increase in the mean wind speed, the fitting degree of each model gradually becomes worsened, which was different from the conclusion obtained in offshore areas.

In summary, the higher the mean wind speed in offshore areas, the better the fitting degree of each wind profile model. In the low wind speed intervals of 8–25 m s^{-1}, the D-H model is the most accurate at describing the observed wind profile, while the log-law model has the lowest fitting degree. When $U(40)$ exceeds 30 m s^{-1}, the log-law model has the highest fitting degree, while the D-H model has the lowest fitting degree. In the onshore area, the higher the mean wind speed is, the lower the fitting degree of each model. In all wind speed intervals, the power-law model has the worst applicability, and the log-law model has the best applicability.

4.2. The Best Applicable Height Range of the Wind Profile Models. Many studies have shown that log-law model is only suitable below a height of 100 m. However, whether the offshore and onshore wind profiles during typhoons in this study are consistent with the above conclusions remains to be explored, and since Section 5 needs to use the wind profile model to fit the observed wind profile to solve the roughness length and power exponent, it is necessary to clarify the best applicable height range of the wind profile model. Therefore, in this study, wind profile models of offshore and onshore strong winds were fitted in different height ranges, respectively. By comparing the RMSE and R parameters, the height range of the best description degree of each model on the observed wind profile was obtained.

For the strong wind profiles of the Mangkhut observed in offshore areas, four wind profile models were fitted to the composite wind profiles in the height ranges of 40–70 m, 40–80 m, 40–90 m, 40–100 m, 40–110 m, 40–120 m, 40–140 m, 40–170 m, 40–190 m, and 40–210 m. Figure 8 shows RMSE and R between the four model-fitted wind profiles and the observed wind profiles. In general, the fitting effect of four wind profile models deteriorated gradually with increasing height. Above 100 m, the error between the model-fitted profiles and observed increased significantly. In detail, the power-law model had a higher degree in the height range of 40–80 m, while the log-law model had a higher degree in the height range of 40–70 m.

For the strong wind profiles of the Lekima observed in onshore area, four wind profile models were fitted to the composite wind profiles in the height ranges of 40–70 m, 40–100 m, 40–130 m, 40–150 m, 40–180 m, 40–200 m, 40–230 m, 40–250 m, and 40–270 m. Figure 9 shows RMSE and R between the four model-fitted wind profiles and the observed wind profiles. All four models had the smallest RMSE and the largest R in the height range of 40–70 m. As the height increased, both RMSE and R changed significantly, and the error between the model-fitted wind speed profile and the observed wind profile gradually increased. The above analysis shows that the four wind profile models have the best applicability in the height range of 40–70 m in onshore areas.

5. Power Exponent Variation of Typhoon Processes

5.1. The Effect of Mean Wind Speed on Power Exponent. The power-law model is the most popular pattern to describe the vertical distribution of wind speed in the wind resistance codes and standards of many countries, due to its simple form [28, 29]. The power exponent α is an important parameter reflecting the variation in the mean wind speed with height. Therefore, it is necessary to study the influencing factors of the power exponent. In Section 4.2, it has been analyzed that the best applicable height ranges of the power-law model in offshore and onshore areas were 40–80 m and 40–70 m, respectively. Therefore, when analyzing the power exponent in this study, the 10-minute mean wind profiles within the height ranges of 40–80 m and 40–70 m were selected to perform the best power law fitting in offshore and onshore areas, respectively. Figure 10 shows the change rule of the power exponent in offshore and onshore areas with $U(40)$. In offshore areas, with increasing mean wind speed, the mean power exponent had a gentle trend and no obvious change. In detail, the mean power exponent decreased slightly from 0.1072 to 0.0934 in the interval of 8–25 m s^{-1} wind speed, and increased slightly to 0.0959 after exceeding 25 m s^{-1}, which was somewhat different with the analysis results of Ishizaki and Aerodynamics [18]. In the onshore area, when $U(40)$ was in the interval of 8–25 m s^{-1} wind speed, the power exponent did not change significantly and was less affected by the mean wind speed, but when $U(40)$ exceeded 25 m s^{-1}, the mean power exponent decreased from 0.3269 to 0.2084. The reason for this change may be

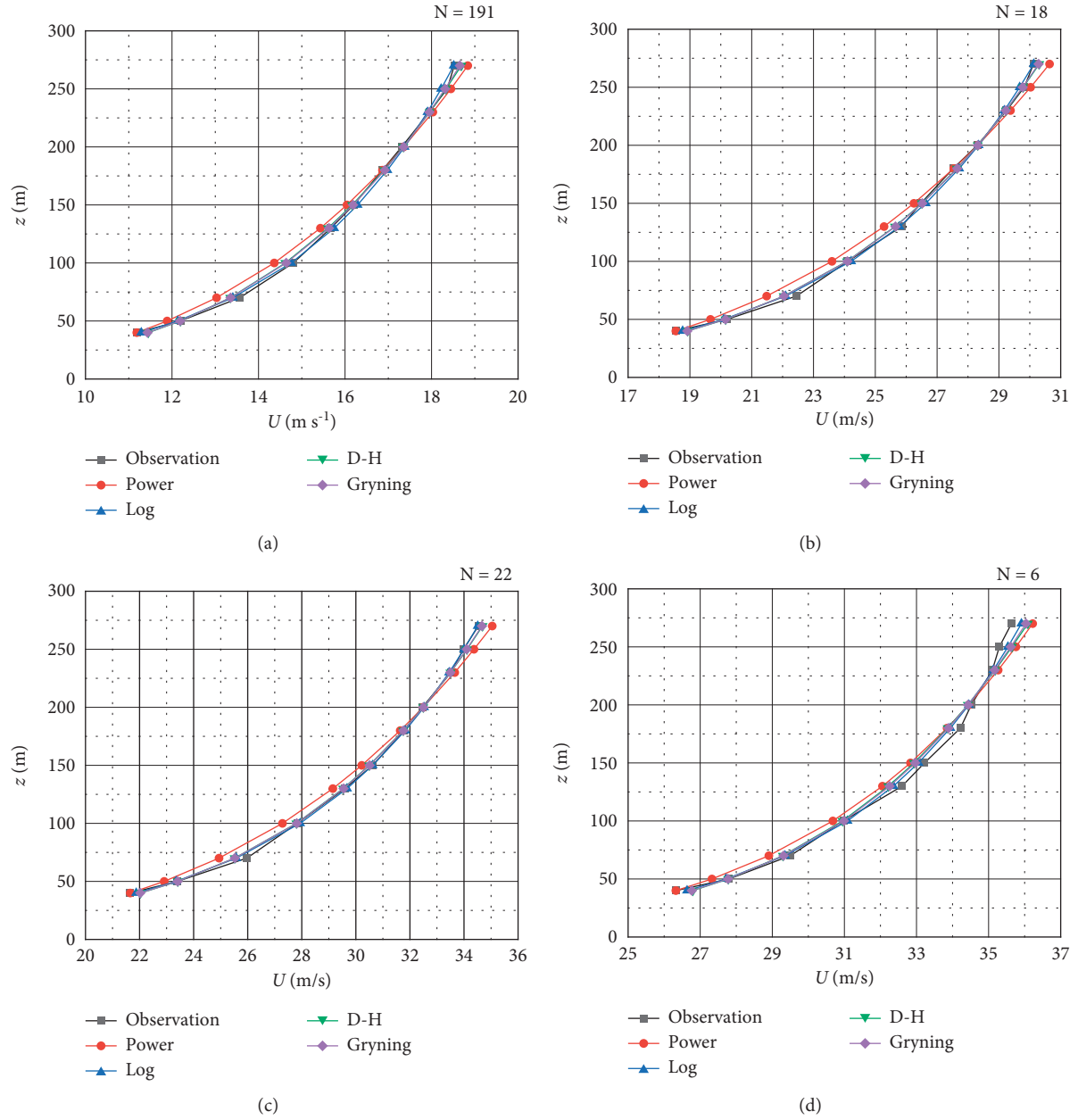

Figure 6: Mean wind profiles by U (40) group, compared with model-fitted wind profiles in typhoon Lekima. Intervals of U (40): (a) 8–17.2 m s^{-1}; (b) 17.2–20 m s^{-1}; (c) 20–25 m s^{-1}; (d) 25–30 m s^{-1}; and (e) 30–35 m s^{-1}.

that there are fewer samples in the wind speed interval of 25–30 m s^{-1}, which is a similar reason that the wind profile models have a poor fitting degree in the wind speed interval of 25–30 m s^{-1} when analyzing the wind profile in the onshore area in Section 4.1. In addition, within the same wind speed interval, the power exponent of the onshore wind profile was much larger than that in the offshore area. For example, in the wind speed interval of 17.2–20 m s^{-1}, the mean power exponent in the offshore area was 0.1071, and the mean power exponent in the onshore area was 0.3453, which is approximately 3.2 times that in the offshore area.

5.2. The Relationship between Roughness Length and Power Exponent. In the neutral steady state of strong wind, the vertical variation of the mean wind speed in the near-surface layer is controlled by the roughness length of the underlying surface [9]. To explore the relationship between the power exponent and roughness length, Panofsky and Dutton [19] pointed out that the relationship between the power exponent and roughness length could be expressed as

$$\alpha = \frac{1}{\ln\left(\sqrt{z_1 z_2}/z_0\right)}, \tag{9}$$

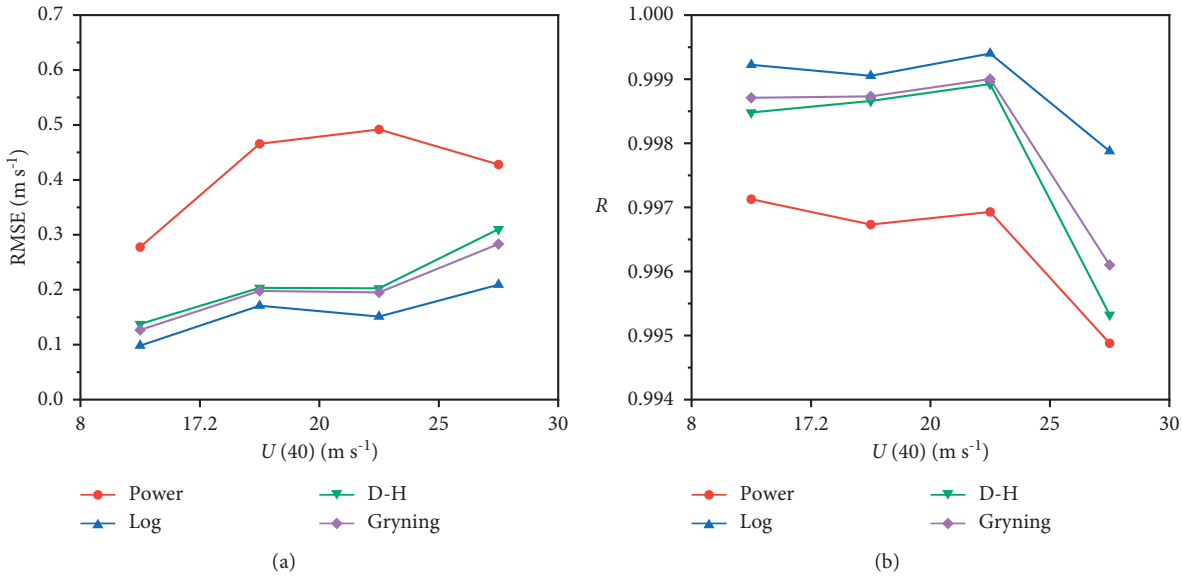

Figure 7: The error between the observed gradient wind speed value and the model-fitted gradient wind speed value by U (40) group in typhoon Lekima.

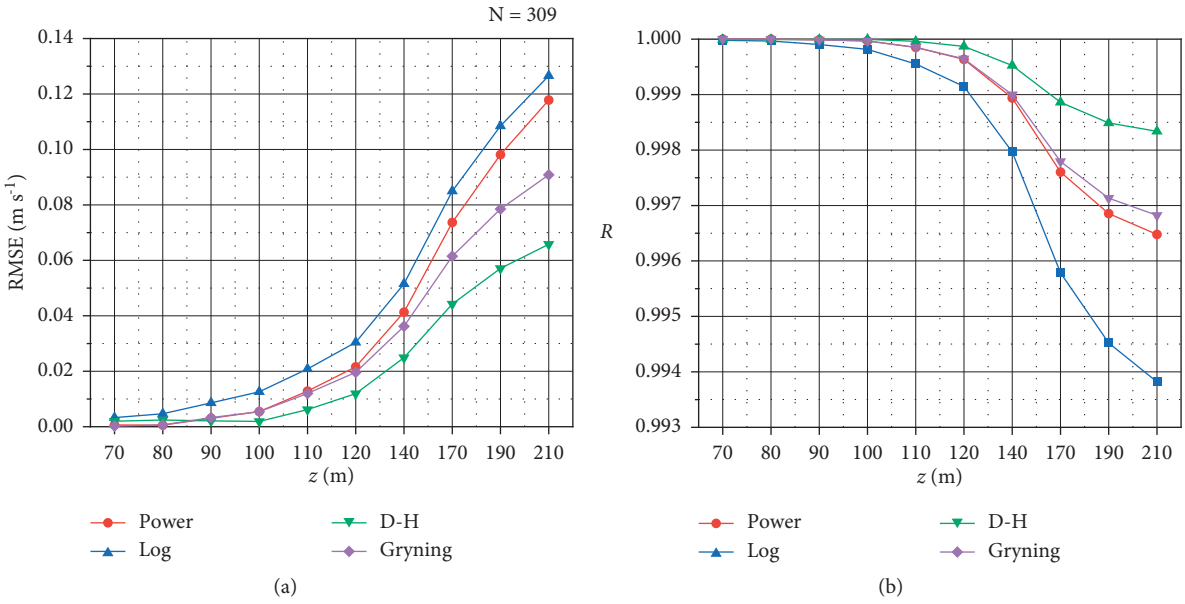

Figure 8: The error between the observed gradient wind speed value and the model-fitted gradient wind speed value in different altitude intervals in typhoon Mangkhut. The horizontal axis represents the upper limit of the height intervals, the lower limit is 40 m height.

where z_1 and z_2 are the lowest and highest heights of the observed value, respectively.

However, since the application of equation (9) requires the use of gradient wind speed data within a certain height range; in practical applications, local observed wind profile data may be lacking. To make the power exponent estimation method based on roughness length simple and effective, Song et al. [20] proposed an empirical formula of the power ratio based on wind records of landfall typhoons on six observation towers. It is expressed as:

$$\alpha = az_0^b. \tag{10}$$

In the formula, a and b are empirical parameters, and z_0 is in centimeters. By fitting multiple typhoon data, Song et al.

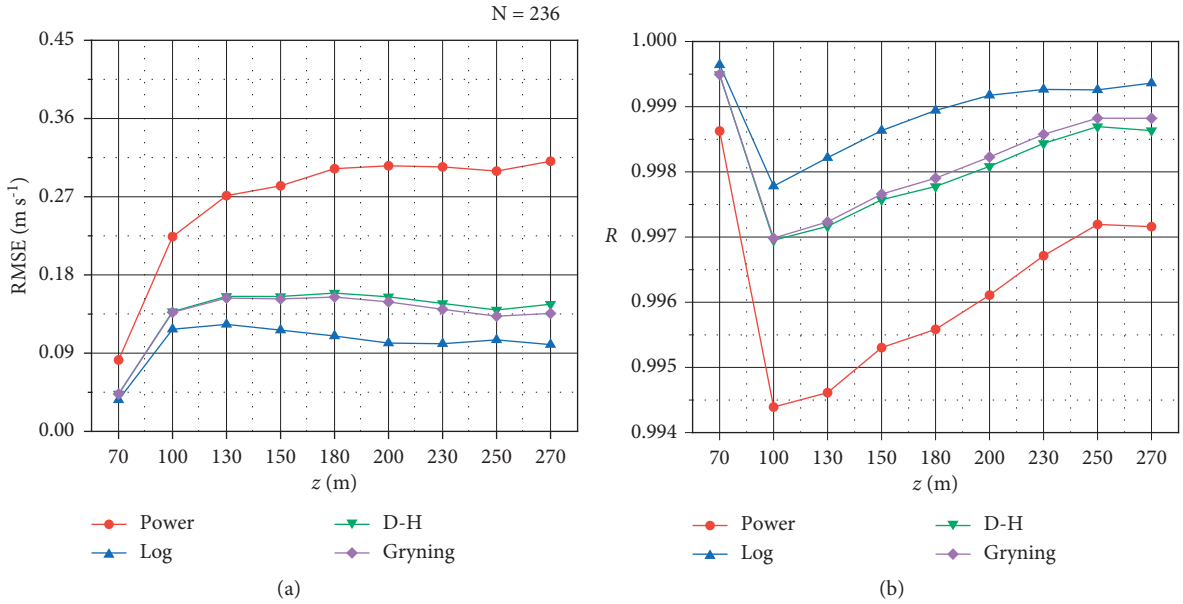

Figure 9: The error between the observed gradient wind speed value and the model-fitted gradient wind speed value in different altitude intervals in typhoon Lekima. The horizontal axis represents the upper limit of the height intervals, the lower limit is 40 m height.

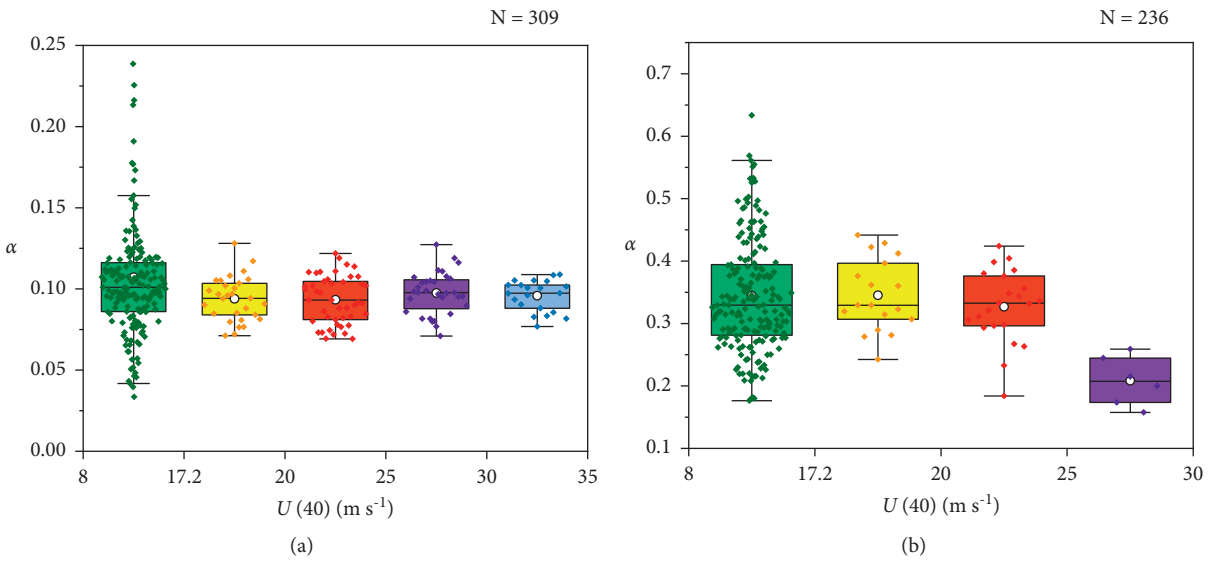

Figure 10: The power law exponent with $U(40)$, including (a) typhoon Mangkhut; (b) typhoon Lekima.

[20] suggested $a = 0.11$ and $b = 0.2$ under typhoon conditions, and $a = 0.11$ and $b = 0.22$ under nontyphoon conditions. He et al. [23] used the Mangkhut data observed by the Shenzhen Meteorological Tower to fit z_0 and α using equation (10), and the fitting results were $a = 0.11$ and $b = 0.18$.

To verify the applicability of this formula in offshore observation sites and over different onshore observation sites, the relationship between the power exponent and roughness length was investigated using Mangkhut and Lekima wind data observed in offshore and onshore sites, respectively. Figure 11 shows the variation rule of the power exponent with roughness length. The power exponent and roughness length z_0 were calculated using equations (1) and (3) offshore and onshore, respectively. In offshore areas, the least squares method was first applied to the wind profiles in the height range of 40–80 m using equation (3), and then the wind profiles with the average residual sum of squares (ARSS) less than or equal to 0.002 m^2/s^2 were selected as samples. Then, the power exponent and z_0 were calculated in the offshore area using equations (1) and (3), respectively. In the onshore area, the least squares method was first fitted to the strong wind profiles in the height range of 40–70 m using equation (3), and then wind profiles with the ARSS less than or equal to 0.01 m^2/s^2 were selected as samples. Then, the power exponent and z_0 were calculated in the onshore area

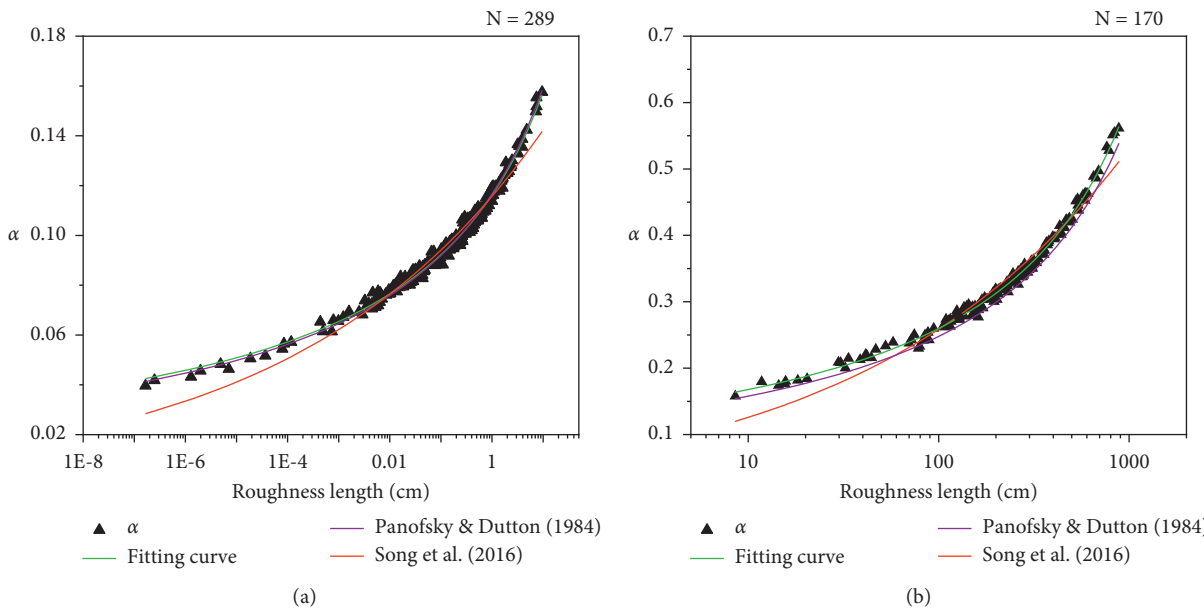

Figure 11: Variation in the power law exponent with roughness length in offshore and onshore areas, and the fitting curves of three models, including (a) typhoon Mangkhut and (b) typhoon Lekima.

Table 2: Fitting results of three power exponential models in offshore and onshore areas.

Model	Observation position	Typhoon name	a	b	Residual variances	F test value	Fa (0.01)
Panofsky and Dutton (1984)	Offshore	Mangkhut	—	—	$3.5952e-6$	31678	6.724
	Onshore	Lekima	—	—	$2.5237e-4$	3963	6.7882
Song et al. (2016)	Offshore	Mangkhut	0.1157	0.0899	$1.2156e-5$	9223	6.724
	Onshore	Lekima	0.0613	0.3127	$2.3982e-4$	4645	6.7882
New model	Offshore	Mangkhut	8.7109	0.0014	$3.3169e-6$	32587	6.724
	Onshore	Lekima	8.5846	0.0085	$3.3402e-5$	32274	6.7882

using equations (1) and (3), respectively. It can be observed that the power exponent increased with increasing roughness length for both offshore and onshore cases, and that the models proposed by Panofsky and Dutton [19] and He et al. [20] were good at characterizing the relationship between the power exponent and z_0. Table 2 shows the fitting parameters and reliability level. The results show that, for the model proposed by [19], the F test values of typhoons in offshore and onshore areas were 31678 and 3963, respectively, which were larger than the values of F (6.724 and 6.7882, respectively) at the 0.01 level of significance. The residual variances were just $3.5952e-6$ and $2.5237e-4$, respectively. For the model proposed by [20], the least square method is used to fit the power exponent and roughness length in this study by using equation (10), the F test values of typhoons in offshore and onshore areas were 9223 and 4645, respectively, which were larger than the values of F (6.724 and 6.7882, respectively) at the 0.01 level of significance. The residual variances were just $1.2156e-5$ and $2.3982e-4$, respectively. The a values were 0.1139 and 0.0613, and the b values were 0.0921 and 0.3127, respectively, which are different from the fitting results in Song et al. [20] and He et al. [23]. The reason is that the power exponent of the fitting in this study used 40 m height as the reference height, while Song et al. [20] and He et al. [23] both used 10 m height as the reference height. However, by observing Figure 11 and comparing the residual variances, it was found that there was some deviation between the distribution of the power exponent obtained by fitting the two models and the actual power exponent. Therefore, a new power exponent model is proposed in this study, as shown below:

$$\alpha = \frac{1}{a - \ln z_0} + b, \tag{11}$$

where α is the power law exponent, a and b are the fitting parameters, z_0 is the roughness length, and the unit is centimeters.

Based on equation (11) and the previously fitted power exponent and z_0 values, the empirical formulae for the power exponent in offshore and onshore areas were obtained in this study. Figure 11 also shows the fitted curves of the new model, and it can be seen that the fit between the new model and the actual power exponent was significantly better than the other two models. Table 2 also presents the fitting parameters and reliability level of the new model. The F test values in offshore and onshore areas were 32587 and 32274, respectively, far greater than the values of F (6.724 and

6.7882, respectively) at the 0.01 level of significance, and the residual variances were $3.3169e-6$ and $3.3402e-5$. By comparing the residual variances, it can be found that the residual variances of the new model were reduced by about 7.41% and 72.71% for the offshore area and about 86.76% and 86.07% for the onshore areas, respectively, compared to the other two modes. The above results can indicate that the model proposed in this study had better applicability. In addition, it can be seen that the applicability of the three models in offshore areas was better than that in the onshore area. The possible reason is that the underlying surface of land is rough and unevenly distributed, and the frequency of wind profile changes with the underlying surface is high, resulting in the distribution of the power exponent being relatively discrete.

6. Conclusion

To compare the difference of offshore and onshore near-surface wind profiles during typhoon and analyze the applicability of four wind profile models including power law, logarithmic law, D-H, and Gryning in offshore and onshore areas. This paper investigated the characteristics of the mean wind profiles for different wind speed intervals based on the wind records of Super Typhoons Mangkhut and Lekima from both offshore and onshore observation sites. Then, the applicability of the power-law model, log-law model, D-H model, and Gryning model in different wind speed intervals and different height ranges was evaluated. Finally, the variation pattern of the power exponent with the mean wind speed and the roughness length was analyzed. Based on the comparison with previous studies and models, a new model describing the relationship between the power exponent and roughness length was proposed. The conclusions are as follows:

(1) In offshore and onshore areas, the normalized wind profiles in different wind speed ranges had different variation trends. In offshore areas, the variation trend of the normalized wind speed profile in the wind speed interval of 8–17.2 m s^{-1} was obviously different from that in other high wind speed intervals. In the onshore area, however, the normalized wind profiles differed less between the three wind speed intervals within 8–25 m s^{-1}, while the normalized wind profiles changed significantly when $U(40)$ was greater than 25 m s^{-1}. With increasing mean wind speed, the change rate of the wind speed ratio with height decreased gradually in offshore and onshore areas. In the same wind speed interval and at the same height, the wind speed ratio in the onshore area was much larger than that in the offshore area.

(2) The applicability of the four wind profile models in offshore areas was significantly affected by the mean wind speed, but the impact in onshore areas was not significant. In the intervals of 17.2–30 m s^{-1} wind speed below 210 m above sea level, with the increase in mean wind speed, the fitting degree of the four wind profile models on the observed wind profile became increasingly better. In addition, the D-H model fits best in the 8–25 m s^{-1} wind speed interval, while the log-law model became the best fit when $U(40)$ is greater than 30 m s^{-1}. Below a height of 270 m above land, there was no obvious trend in the fit of the four wind profile models to the observed wind profile as the mean wind speed increased. In different wind speed intervals, the log-law model had the highest fitting degree, while the power-law model had the lowest fitting degree.

(3) In different height ranges, the fitting degrees of the four wind profile models on the observed wind profile were very different. In offshore areas, in general, the fitting degrees of four models on the observed profiles became progressively lower as the height increased. The power-low model has the highest fitting degree in the height range of 40–80 m. In onshore areas, the four wind profile models had the highest fitting degree on the observed wind profile in the height range of 40–80 m.

(4) In offshore areas, as the mean wind speed increased, the power exponent had a gentle trend and no obvious change. In the onshore area, the power exponent was also less affected by the mean wind speed. In addition, the onshore power exponent was much larger than that offshore in the same wind speed range.

(5) The power exponent increased with increasing roughness length in both offshore and onshore areas. Compared to the models proposed by Panofsky and Dutton [19] and Song et al. [20], the empirical model proposed in this study could better describe the relationship between the power exponents and the roughness length in offshore and onshore areas. The new empirical model was a simple and effective method for accurately estimating the power exponent of the wind speed profile of offshore and onshore typhoons.

The conclusions of this study provided a reference for typhoon near-surface layer modeling in wind tunnel tests and numerical simulations of computational fluid dynamics, and contributed to an enhanced understanding of the differences between offshore and onshore typhoon wind profiles, and provided a reference for the typhoon resistance design of offshore wind turbines and onshore building structures. Finally, the proposed empirical power exponent function provided a simple and effective method for estimating the power exponent from the roughness length in typhoon-prone areas.

This study analyzed only individual typhoons observed in offshore and onshore areas. In the future, more observation data of typhoons are needed to verify the conclusions drawn in this study, and further promote the theoretical and applied research of wind speed profiles in the near-surface layer under typhoon conditions in wind engineering and meteorology.

Data Availability

Due to the rights of third parties and commercial confidentiality, the data are not freely available.

Conflicts of Interest

The authors declare no possible conflicts of interest.

Acknowledgments

The authors thank the American Journal Experts (AJE) for editing the English text of this manuscript.

References

[1] A. G. Davenport, "Rationale for determining design wind velocities," *Journal of the Structural Division*, vol. 86, no. 5, pp. 39–68, 1960.

[2] E. Buckingham, "On physically similar systems; illustrations of the use of dimensional equations," *Physical Review*, vol. 4, no. 4, pp. 345–376, 1914.

[3] A. Monin and A. Obukhov, "Basic laws of turbulent mixing in the atmosphere near the ground," *Trudy Geofizicheskogo Instituda, Akademiya Nauk SSSR*, vol. 24, no. 151, pp. 163–187, 1954.

[4] B. Brümmer, "Wind shear at tilted inversions," *Boundary-Layer Meteorology*, vol. 57, no. 3, pp. 295–308, 1991.

[5] L. Mahrt, "The influence of momentum advections on a well-mixed layer," *Quarterly Journal of the Royal Meteorological Society*, vol. 101, no. 427, pp. 1–11, 1975.

[6] D. M. Deaves and R. I. Harris, *A Mathematical Model of the Structure of Atrong Winds*, Construction Industry Research and Information Association, London, UK, 1978.

[7] S.-E. Gryning, E. Batchvarova, B. Brümmer, H. Jørgensen, and S. Larsen, "On the extension of the wind profile over homogeneous terrain beyond the surface boundary layer," *Boundary-Layer Meteorology*, vol. 124, no. 2, pp. 251–268, 2007.

[8] W. M. Frank, "The structure and energetics of the tropical cyclone I. Storm structure," *Monthly Weather Review*, vol. 105, no. 1, p. 1, 1977.

[9] M. D. Powell, P. J. Vickery, and T. A. Reinhold, "Reduced drag coefficient for high wind speeds in tropical cyclones," *Nature*, vol. 422, no. 6929, pp. 279–283, 2003.

[10] Y. Tamura, K. Suda, A. Sasaki et al., "Simultaneous wind measurements over two sites using Doppler sodars," *Journal of Wind Engineering and Industrial Aerodynamics*, vol. 89, no. 14-15, pp. 1647–1656, 2001.

[11] X. Wang, P. Huang, and M. Gu, "Variation of wind profiles near ground during typhoon "muifa"," *Journal of Tongji University*, vol. 41, no. 8, pp. 1165–1171, 2013.

[12] L. Li, A. Kareem, J. Hunt et al., "Observed sub-hectometer-scale low level jets in surface-layer velocity profiles of land-falling typhoons," *Journal of Wind Engineering and Industrial Aerodynamics*, vol. 190, pp. 151–165, 2019.

[13] I. M. Giammanco, J. L. Schroeder, and M. D. Powell, "GPS dropwindsonde and WSR-88d observations of tropical cyclone vertical wind profiles and their characteristics," *Weather and Forecasting*, vol. 28, no. 1, pp. 77–99, 2013.

[14] Y. C. He, P. W. Chan, and Q. S. Li, "Wind profiles of tropical cyclones as observed by Doppler wind profiler and anemometer," *Wind and Structures*, vol. 17, no. 4, pp. 419–433, 2013.

[15] AIJ, "Recommendations for loads on buildings," in *AIJ-RLB-2004*Architectural Institute of Japan, Tokyo, Japan, 2004.

[16] ASCE, "Minimum design loads for buildings and other structures," in *ASCE/SEI 7-05*ASCE, Reston, VA, USA, 2006.

[17] China National Standard (GB-50009 2012), *Load Code for the Design of Building Structures*, Ministry of Construction People's Republic of China: China Architecture & Building Press, Beijing, China, 2012, in Chinese.

[18] H. Ishizaki, "Wind profiles, turbulence intensities and gust factors for design in typhoon-prone regions," *Journal of Wind Engineering and Industrial Aerodynamics*, vol. 13, no. 1–3, pp. 55–66, 1983.

[19] H. Panosfsky and J. Dutton, *Atmospheric Turbulence: Models and Methods for Engineering Applications*, John Wiley & Sons, NewYork, NY, USA, 1984.

[20] L. Song, W. Chen, B. Wang, S. Zhi, and A. Liu, "Characteristics of wind profiles in the landfalling typhoon boundary layer," *Journal of Wind Engineering and Industrial Aerodynamics*, vol. 149, pp. 77–88, 2016.

[21] S. M. Tang, Y. Guo, X. Wang et al., "Validation of Doppler wind lidar during super typhoon Lekima (2019)," *Frontiers of Earth Science*, 2020.

[22] J. Wieringa, "Representative roughness parameters for homogeneous terrain," *Boundary-Layer Meteorology*, vol. 63, no. 4, pp. 323–363, 1993.

[23] J. Y. He, Y. C. He, Q. S. Li et al., "Observational study of wind characteristics, wind speed and turbulence profiles during Super Typhoon Mangkhut," *Journal of Wind Engineering and Industrial Aerodynamics*, vol. 206, Article ID 104362, 2020.

[24] W. Chen, L. Song, S. Zhi, H. Huang, and P. Qin, "Analysis on gust factor of tropical cyclone strong wind over different underlying surfaces," *Science China Technological Sciences*, vol. 54, no. 10, pp. 2576–2586, 2011.

[25] J. L. Franklin, M. L. Black, and K. Valde, "GPS dropwindsonde wind profiles in hurricanes and their operational implications," *Weather and Forecasting*, vol. 18, no. 1, pp. 32–44, 2003.

[26] Y. Tamura, Y. Iwatani, K. Hibi et al., "Profiles of mean wind speeds and vertical turbulence intensities measured at seashore and two inland sites using Doppler sodars," *Journal of Wind Engineering and Industrial Aerodynamics*, vol. 95, no. 6, pp. 411–427, 2007.

[27] P. J. Vickery, D. Wadhera, M. D. Powell, and Y. Chen, "A hurricane boundary layer and wind field model for use in engineering applications," *Journal of Applied Meteorology and Climatology*, vol. 48, no. 2, pp. 381–405, 2009.

[28] Y. Ge, X. Jin, and S. Cao, "Comparison of APEC wind loading codification and revision of Chinese National Code," in *Proceedings of the 6th Workshop on Regional Harmonization of Wind Loading and Wind Environmental Specifications in Asia-Pacific Economies*, Gangneung, Korea, October 2010.

[29] M. Yoshida, M. Yamamoto, K. Takagi, and T. Ohkuma, "Prediction of typhoon wind by level 2.5 closure model," *Journal of Wind Engineering and Industrial Aerodynamics*, vol. 96, no. 10-11, pp. 2104–2120, 2008.